The Interpretation of Remotely Sensed High Cloud Emittances

C. M. R. PLATT AND G. L. STEPHENS[1]

CSIRO Division of Atmospheric Physics, Mordialloc, Victoria, Australia 3195

(Manuscript received 10 March 1980, in final form 17 June 1980)

ABSTRACT

The scattering and reflection components of the remotely measured effective beam emittance of high clouds are calculated using a detailed model of radiative transfer through cirrus. Two atmospheric profiles of temperature and humidity are used representing tropical and midlatitude summer atmospheres respectively. The scattering and reflection components of the measured beam emittance are shown to be appreciable, particularly for tropical atmospheres where for example the reflection component at the ground for vertical viewing is 20% of the total emittance.

Computed values of the broad-band effective flux emittance are compared with equivalent values of the narrow-band effective flux emittance at 11 μm wavelength and the narrow-band beam emittance at 11 μm. It is shown that the two former quantities are well correlated and approximately equal in magnitude.

1. Introduction

High cirrus clouds are important radiatively because they are cold clouds which reduce the radiation loss to space typically by 20–30%.

The inherent problems in obtaining optical properties of high clouds from remote radiometric measurements have been considered by a number of authors (e.g., Shenk and Curran, 1973; Reynolds and Vonder Haar, 1977; Platt, 1979).

There are two main problems connected with remote measurements: first, the cloud scatters as well as emits infrared radiation and, second, a remote radiometer measures a radiance in a narrow band of wavelengths rather than a total broad-band flux.

If upward (or downward) radiances are measured from above (or below) a cloud then an *effective* emittance can be calculated in terms of these radiances (provided that the cloud temperature is also known) (Cox, 1976). Generally, the upward and downward effective emittances are not equal because the measured radiances contain components of reflected and scattered radiation as well as emitted radiation. The effective emittance is thus in general different from the true "absorption" emittance of the cloud. If the effects of reflection and scattering are neglected, which has often been the case in the past, the calculated absorption emittance can be in error by up to 20%. The first object of this article is to provide magnitudes for the scattering and reflection components of the calculated emittance. These are computed here using the detailed radiative transfer scheme of Stephens (1980), and assuming ice crystals to be approximated by long cylinders of appropriate dimensions. To aid in the interpretation of the results a simple conceptual model is employed which gives the reflection and scattering components as additional terms to the conventional equation for emittance. Because cloud temperature is obtained variously from observations as either the cloud top, mid-cloud or cloud base temperature, the effects of these various definitions on the calculated effective emittances are also considered.

To be useful for incorporation into climate and dynamic models (e.g., Stephens and Webster, 1979), the deduced absorption emittances must be converted into broad-band flux emittances. Remotely sensed emittances are usually made in a narrow band of wavelengths within the atmospheric window. The 11 μm band is standard for meteorological satellites and has been used extensively also for ground-based measurements. One problem, then, is how the narrow-band emittance can be related to the broad-band emittance. As mentioned previously, a further difficulty is that remote radiometers measure a directional radiance. This radiance then has to be interpreted in terms of a radiant flux. An approximate relation between flux emittance and beam emittance has been given previously by Platt and Dilley (1979), but this expression was derived by neglecting scattering. The second object of this article is to provide accurate relations between the narrow-band beam

[1] Temporary affiliation: Department of Atmospheric Sciences, Colorado State University, Fort Collins 80523.

0022-4928/80/102314-09$06.25

and flux emittances and the broad-band flux emittance and these are calculated here for various latitudes and cloud temperatures.

2. Theory

Consider a cloud as shown in Fig. 1. The radiances are incident and exiting on the cloud at some angle θ. This is implied in the following sections but the θ suffix is excluded for convenience. Subscripts 1 and 2 refer to radiances at the top and bottom cloud boundaries, respectively. Subscripts 5 and 6 refer to effective radiances scattered into the beam in the upward and downward directions, respectively. The plus and minus superscripts refer respectively to radiances in the upward and downward directions. The radiances and other quantities in this section are assumed to be for a wavelength of 11 μm. The narrow-band effective upward and downward beam emittances are then defined as

$$\epsilon_{e\lambda}\uparrow = \frac{L_2^- - L_1^-}{L_2^- - L_B(T)}, \quad (1)$$

$$\epsilon_{e\lambda}\downarrow = \frac{L_2^+ - L_1^+}{L_B(T) - L_1^+}, \quad (2)$$

where $L_B(T)$ is the cloud blackbody radiance at some temperature T. The λ subscripts distinguish the narrow-band from the broad-band emittance.

A conceptual model is now given which considers the separation of reflection and multiple scattering from absorption in the equations. This model is useful for visualizing the forms of the components of reflection and scattering which can be computed from the detailed radiative transfer model. The reflectance of the cloud for incident beam radiation is defined as ρ. Upward radiances below cloud base which are incident on the cloud at all angles between 0 and 90° are partially reflected into the downward beam at an angle θ. The radiance in the direction of L_2^+ due to this reflection is defined as $\rho' L_2^+$. In general, ρ' will not be equal to ρ because the radiances incident at the cloud boundary vary with the angle of incidence. For this reason also the ρ' at cloud top may be different from the ρ' at cloud base. However, for convenience, they are considered to be equal so that the downward radiance reflected into the direction of L_1^- at cloud top is defined as $\rho' L_1^+$. Of the radiance L_2^- which enters the cloud, a fraction $\epsilon_{a\lambda}$ is absorbed, ρ is reflected down, and γ is scattered out of the beam within the cloud. An effective amount γL_5 is scattered *into* the beam. The total upward radiance at the top is then

$$L_1^- = \rho' L_1^+ + (1 - \epsilon_{a\lambda} - \rho - \gamma)L_2^- + \gamma L_5 + L_B(T)\epsilon_{a\lambda}, \quad (3)$$

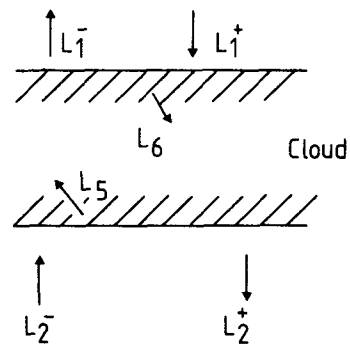

FIG. 1. A schematic depiction of the different radiances from and within the cloud.

where $L_B(T)$ is the blackbody radiance at an effective temperature T. Similarly, the total downward radiance at the cloud base is

$$L_2^+ = \rho' L_2^- + (1 - \epsilon_{a\lambda} - \rho - \lambda)L_1^+ + \gamma L_6 + L_B(T)\epsilon_{a\lambda}. \quad (4)$$

The equations for sensing from a satellite and from the ground are now considered separately. It is assumed that corrections have been made for the effects of the intervening atmosphere, and that for the case of ground-based sensing there is no intervening middle- or low-level cloud.

a. Satellite sensing

Rearrangement of Eq. (3) gives

$$\epsilon_{a\lambda} = \frac{L_2^- - L_1^-}{L_2^- - L_B(T)} - \frac{(\rho L_2^- - \rho' L_1^+)}{[L_2^- - L_B(T)]} - \gamma\left[\frac{L_2^- - L_5}{L_2^- - L_B(T)}\right]. \quad (5)$$

Eq. (5) can be abbreviated to

$$\epsilon_{a\lambda}\uparrow = \epsilon_{e\lambda}\uparrow - \epsilon_{\rho\lambda}\uparrow - \epsilon_{\gamma\lambda}\uparrow, \quad (6)$$

where $\epsilon_{\rho\lambda}\uparrow = (\rho L_2^- - \rho' L_1^+)/[L_2^- - L_B(T)]$ is the term representing the reflection components and $\epsilon_{\gamma\lambda}\uparrow = \gamma(L_2^- - L_5)/[L_2^- - L_B(T)]$ is the term representing the multiple-scattering components. For high clouds and in the atmospheric window, L_1^+ is effectively zero. $\epsilon_{\rho\lambda}\uparrow$ is dependent on the transmitted radiances L_2^- and on $L_B(T)$, and cannot be separated computationally from the term $\epsilon_{\gamma\lambda}\uparrow$. Hence a term $\epsilon'_{\gamma\lambda}\uparrow$ will be calculated where $\epsilon'_{\gamma\lambda}\uparrow = \epsilon_{\rho\lambda}\uparrow + \epsilon_{\gamma\lambda}\uparrow$.

b. Ground-based sensing

The equivalent expression to Eq. (5) for the emittance measured below the cloud is (where L_2^+ is the total radiance exiting from the cloud base)

$$\epsilon_{a\lambda} = \frac{L_2^+}{L_B(T)} - \rho' \frac{L_2^-}{L_B(T)} - \frac{\gamma L_6}{L_B(T)} \quad (7)$$

$$= \epsilon_{e\lambda}\downarrow - \epsilon_{\rho\lambda}\downarrow - \epsilon_{\gamma\lambda}\downarrow, \quad (8)$$

where L_1^+ is again zero. Then the second term depends only on reflected radiation and it can thus be calculated separately.

c. Relation between slant emittance and vertical emittance

If the quantity $\epsilon_{a\lambda}$ is measured at a zenith angle θ, then it is convenient to convert $\epsilon_{a\lambda}(\theta)$ to an equivalent vertical value $\epsilon_{a\lambda}(0)$. If $\delta_{a\lambda}(\theta)$ is the *absorption* optical depth through the slant path at angle θ (i.e., scattering effects have been subtracted) then

$$\delta_{a\lambda}(0) = \delta_{a\lambda}(\theta) \cos\theta, \quad (9)$$

$$\epsilon_{a\lambda}(0) = [1 - \exp - (\delta_{a\lambda}(\theta) \cos\theta)]. \quad (10)$$

But

$$\delta_{a\lambda}(\theta) = - \ln[1 - \epsilon_{a\lambda}(\theta)], \quad (11)$$

so that

$$\epsilon_{a\lambda}(0) = 1 - \exp[\ln(1 - \epsilon_{a\lambda}(\theta) \cos\theta], \quad (12)$$

which reduces to

$$\epsilon_{a\lambda}(0) = 1 - [1 - \epsilon_{a\lambda}(\theta)]^{\cos\theta}. \quad (13)$$

The emittance at emergent angle θ can thus be converted directly into a vertical beam emittance $\epsilon_{a\lambda}(0)$.

d. Definition of emittances

A remote radiometer measures a radiance, leading to a beam absorption emittance $\epsilon_{a\lambda}$. In order to be used for a radiative transfer model, the quantity $\epsilon_{a\lambda}$ must be related to an effective broad-band flux emittance ϵ_e, i.e., covering all wavelengths. This emittance is defined as (e.g., Cox, 1976)

$$\epsilon_e^+ = \frac{M_2^+ - M_1^+}{M_2^+ - \sigma T^4}, \quad (14)$$

$$\epsilon_e^- = \frac{M_1^- - M_2^-}{M_1^- - \sigma T^4}, \quad (15)$$

where the M's are broad-band fluxes (or exitances) equivalent to the L's in Fig. 1 and σ is the Stefan-Boltzmann constant. The narrow-band effective flux emittances $\epsilon_{e\lambda}^+$ and $\epsilon_{e\lambda}^-$ can be defined in a similar manner in terms of equivalent narrow-band fluxes. In general, upward and downward emittances are unequal because of the effects of scattering and, in the broad-band case, the different spectral compositions of the various fluxes.

If scattering effects are neglected then there is a simple relationship between the narrow-band flux (absorption) emittance $\epsilon_{a\lambda}^F$ and the beam emittance $\epsilon_{a\lambda}$. This is given by (Platt and Dilley, 1979):

$$\epsilon_{a\lambda}^F = \frac{\int_0^{\pi/2} \{1 - \exp[-\delta_a(0) \sec\theta]\} \cos\theta d(\cos\theta)}{\int_0^{\pi/2} \cos\theta d(\cos\theta)}. \quad (16)$$

In practice, Eq. (16) will not be accurate because of scattering effects but, nevertheless, it is a useful guide to the relation between flux and beam emittance. The relations between $\epsilon_{a\lambda}^F$, $\epsilon_{e\lambda}^+$ and $\epsilon_{e\lambda}^-$ are discussed later.

For low water clouds the narrow-band flux emittance $\epsilon_{e\lambda}$, for wavelengths in the atmospheric window, is approximately equal to the broad-band flux emittance ϵ_e. This is due to the fact that the fluxes within the atmospheric absorption bands are close to blackbody at ambient temperature and most of the radiation exchange occurs within the atmospheric window (Paltridge and Platt, 1976). The extent to which this is true for high clouds is not known, and will be investigated here.

3. Cloud model

The cloud particles are assumed to be long ice cylinders, as an approximation to the crystal shapes found in high clouds (Stephens, 1980). To make the calculations more tractable, three types of monodisperse cloud are considered. Their physical properties are shown in Table 1, where σ_E is the extinc-

TABLE 1. Optical properties of the three monodisperse model clouds.

	σ_E (km^{-1})	$\tilde{\omega}_0$	$<\cos\theta>$
Case 1	0.836	0.5249	0.702
Case 2	2.579	0.5104	0.7864
Case 3	13.198	0.6390	0.814
Case 1	l = 300 μm, r = 75 μm,	$n(r)$ = 0.0095,	IWC* = 0.05 g m^{-3}
Case 2	l = 100 μm, r = 25 μm,	$n(r)$ = 0.25,	IWC = 0.05 g m^{-3}
Case 3	l = 200 μm, r = 5 μm,	$n(r)$ = 32,	IWC = 0.05 g m^{-3}

* Ice (or liquid) water content of cloud.

tion coefficient, $\tilde{\omega}_0$ the single-scattering albedo, $\langle\cos\theta\rangle$ the asymmetry parameter, l the crystal length, r the radius, $n(r)$ the number density and IWC the ice water content. Note that as the IWC is held constant, the particle size and thus the value of σ_E (hence the optical depth) of the cloud vary between the three models. Two model atmospheres are considered, one representing a tropical situation and the other, a midlatitude summer situation. The temperature and humidity profiles for these atmospheres are given in by McClatchey *et al.* (1972).

The single-scattering properties of each cloud model are discussed by Stephens (1980).

4. The radiative transfer model

The multiple-scattering radiative transfer model employed in this study has been described elsewhere (Stephens, 1976, 1978). In the model the atmosphere is divided into N layers of varying thickness and $N + 1$ levels. Cloud is inserted into a number of adjacent layers, each with a different temperature. In order to obtain a range of cloud optical depths, each of these layers is then treated as a separate cloud.

Stephens (1980) emphasized that the solution to the radiative transfer model, in radiance (and flux) form, could be separated into two distinct components via

$$\left.\begin{aligned} L^+_{n+1} &= \rho(1, n+1)L^-_{n+1} + V^+_{n+1/2} \\ L^-_n &= \tau(n, n+1)L^-_{n+1} + V^-_{n+1/2} \end{aligned}\right\}, \qquad (17)$$

where $\rho(l,n+1)$ and $\tau(n,n+1)$ are the diffuse reflection and transmission operators, L^+_{n+1} is the downward radiance vector at cloud base (i.e., essentially L^+_2 in Fig. 1) and L^-_n is similarly the upward radiance vector at cloud top (L^-_1). The levels are numbered from $n = 1$ to $N + 1$ downward from the top of the atmosphere. Eq. (17) suggests that the resultant radiances at cloud base are composed of a reflection contribution $[\rho(l, n+1)L^-_{n+1}]$ and a term $V^+_{n+1/2}$ which contains multiple-scattering and emission contributions. Similarly, the upward radiance at cloud top consists of a transmitted component $[\tau(n, n+1)L^-_{n+1}]$ and a term $V^-_{n+1/2}$ which contains multiple-scattering, emission and reflection contributions. Since we assume that the downward radiance at cloud top is zero, we set the reflectance contribution in $V^-_{n+1/2}$ to zero [for more details see Stephens (1980)].

Thus the solutions provided by the multiple-scattering model given by (17) can be directly related to the conceptual models described by (3) and (4). Matching terms from (17) and (3) and (4) produces

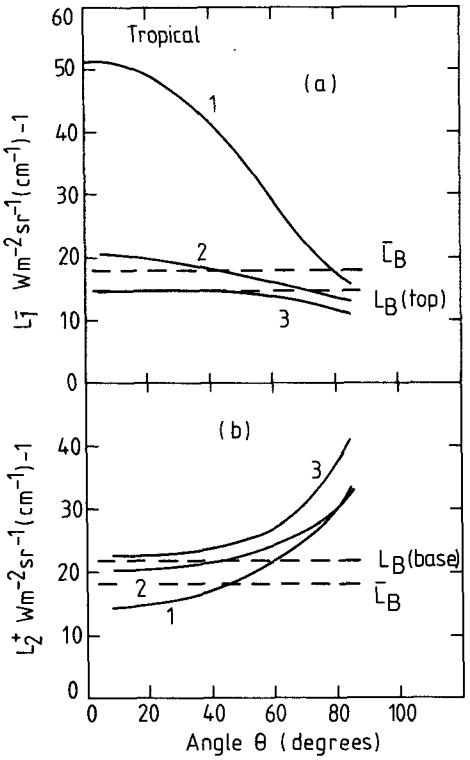

FIG. 2. Exitant radiances L^-_1 and L^+_2 as a function of emergent angles from a cirrus cloud imbedded in a model tropical atmosphere. Curves 1, 2 and 3 refer to radiances determined from the scattering properties in Table 1 as cases 1, 2 and 3, respectively, and for $\lambda = 11$ μm.

$$\left.\begin{aligned} V^+_{n+1/2} &\approx L_6 + L_B(T)\epsilon_{a\lambda} \\ V^-_{n+1/2} &\approx \gamma L_5 + L_B(T)\epsilon_{a\lambda} \\ \rho(1, n+1)L^-_{n+1} &\approx \rho' L^-_2 \\ \tau(n, n+1)L^-_{n+1} &\approx (1 - \epsilon_{a\lambda} - \rho - \gamma)L^-_2 \end{aligned}\right\}, \qquad (18)$$

again for $L^+_1 = 0$.

A knowledge of $\epsilon_{a\lambda}$ [determined from (10) using the single-scattering absorption optical depth $\delta_{a\lambda}$] and $L_B(T)$ can provide an estimation of the multiple-scattering contributions γL_6 and γL_5 by way of the first two equations of (18) and computation of $V^+_{n+1/2}$ and $V^-_{n+1/2}$ from the detailed transfer model Stephens (1980). In this way, as mentioned previously, the simple conceptual model described above can be employed to interpret the solutions of the more complex multiple-scattering model and to provide estimates of the reflection and multiple-scattering effects on emergent radiance fields and thus emittances derived from these radiances.

5. Results

The radiances at the cloud boundary are plotted against angle of emergence (zenith angle) in Figs. 2 and 3 for two model atmospheres. The radiances

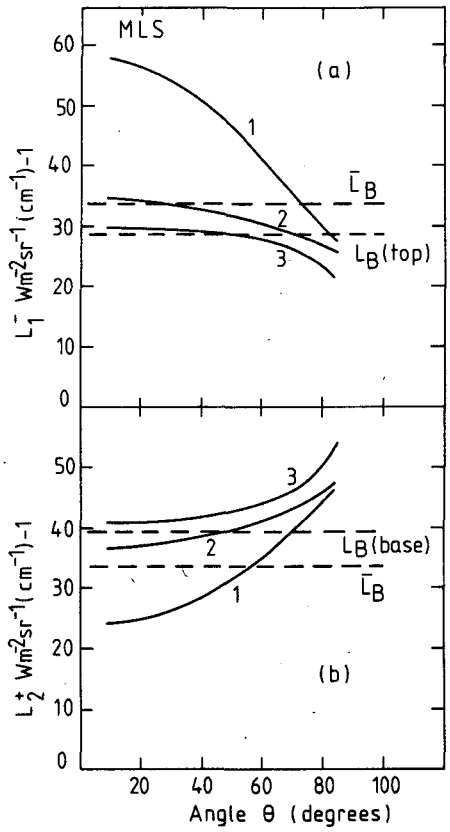

FIG. 3. As in Fig. 2 except for a model midlatitude (summer) atmosphere.

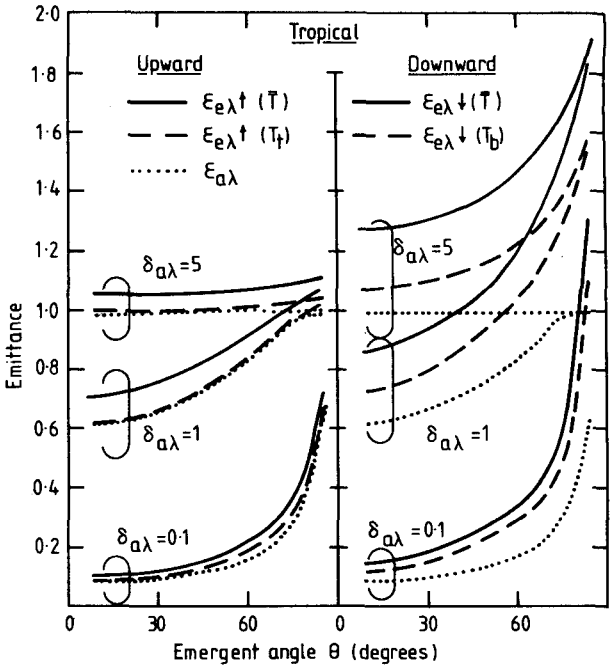

FIG. 5. The 11 μm beam emittance as a function of emergent angle determined for calculations associated with Fig. 2 but with the specified cloud optical depths of 5, 1 and 0.1. Solid curves represent the effective emittance (i.e., includes all scattering effects) determined with the mean cloud temperature; dashed curve is similarly an effective emittance but for the respective boundary temperatures; and the dotted curves are the "absorption emittance" curves (i.e., include contributions only by absorption processes). $T_t - T_b = 11°C$, $\bar{T} = -63°C$.

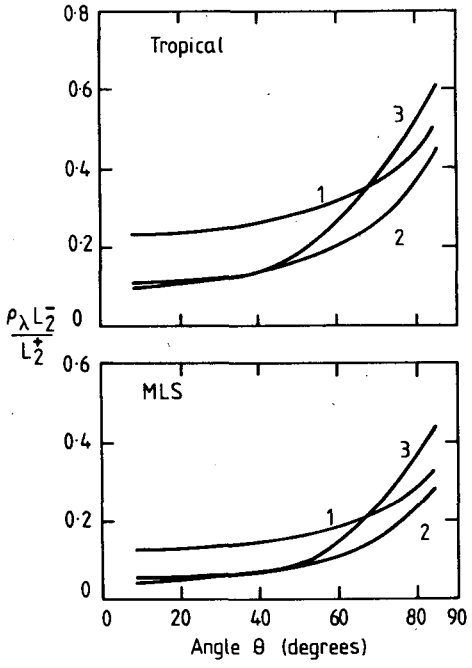

FIG. 4. Fraction of the downward radiation due to cloud reflection for the three case studies listed in Table 1 (i.e., $\rho_\lambda L_2^-/L_2^+$) for λ = 11 μm.

at cloud top include a component of surface radiation, particularly for the case 1 cloud, which is optically thin. The radiances indicate the effects of reflection of upwelling radiation by the cloud, so that at large angles of incidence the cloud-base radiances are greater than the blackbody values at cloud temperature. Thus there is limb brightening at the cloud base. There is a converse effect at cloud top with limb darkening. These effects are similar, but of a larger amplitude, than those found by Yamamoto *et al.* (1970) for water clouds.

The fraction of the downward radiation which is due to cloud reflection is shown in Fig. 4 for various cases. The reflected component is quite appreciable, particularly at large angles, as is also apparent from the limb effects of Figs. 2 and 3.

In Figs. 5 and 6 the emittance $\epsilon_{a\lambda}$ is compared with the values of $\epsilon_{e\lambda}\uparrow$ and $\epsilon_{e\lambda}\downarrow$ as given by Eqs. (1) and (2) and for three optical depths. The radiances in these equations were computed from the detailed radiative transfer model. The effects of using different defined cloud temperatures to calculate the $\epsilon_{e\lambda}$'s are also shown. The difference between the curves at a given emergent angle indicates the correction which has to be applied to the experimental values of $\epsilon_{e\lambda}\uparrow$ and $\epsilon_{e\lambda}\downarrow$ in order to obtain a value of $\epsilon_{a\lambda}$. In all cases, the effective emittances

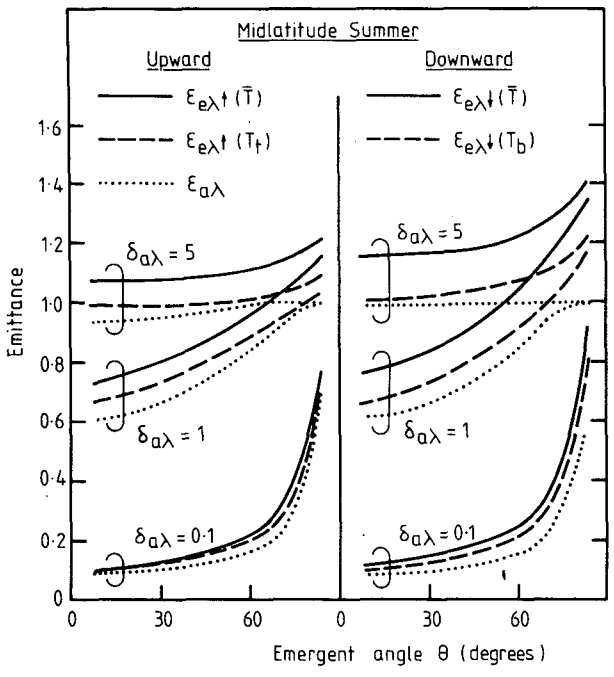

FIG. 6. As in Fig. 5 except for midlatitude summer model atmosphere. $T_t - t_b = 11°C$, $\bar{T} = -38°C$.

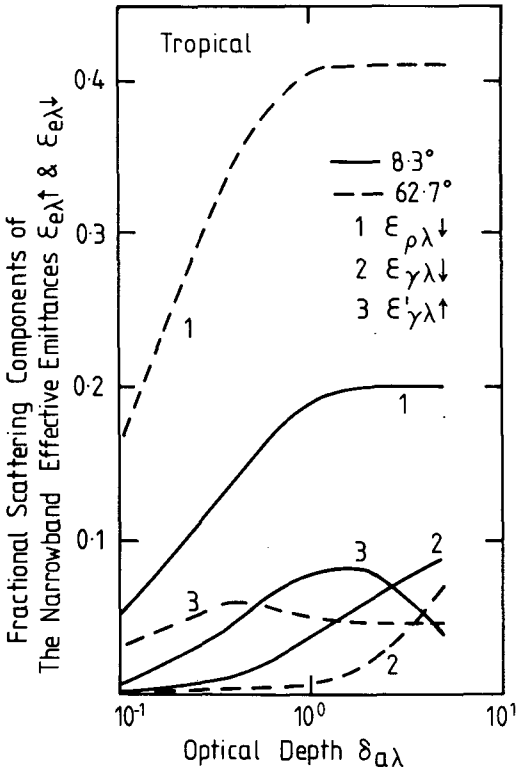

FIG. 7. Fractional scattering components of effective radiance emittance for $\lambda = 11$ μm and for a model tropical atmosphere. That is, the scattering contributions to effective emittance as defined in Eqs. (6) and (8) for radiation emerging at 8.3 and 62.7° as a function of absorption optical depth.

are greater than the absorption emittances. In the case where the optical depth $\delta_{a\lambda}$ is 5, the calculated emittance is generally greater than unity. This is because of the large reflection component. It can be seen that for the upward case, the emittance calculated from the cloud-top temperature is closer to $\epsilon_{a\lambda}$ than when the mid-cloud temperature is used. The same is true for the downward emittance when the cloud-base temperature is used.

Figs. 7 and 8 show, for the case of the downward emittance, the contributions of the two components of scattering, the internal multiple scattering component $\epsilon_{\gamma\lambda}\downarrow$ and the external reflection component $\epsilon_{\rho\lambda}\downarrow$. The combined components in the upward emittance are shown as $\epsilon'_{\gamma\lambda}\uparrow$. The contributions are shown plotted against absorption optical depth $\delta_{a\lambda}$ for two emergent angles. Generally, for the downward emittance, the reflection components are larger than the multiple-scattering components, particularly for slant paths (i.e., larger emergent angles) and for the tropical case.

The upward emittance is also appreciably modified by both multiple scattering within the cloud and reflections from the cloud base. The corrections are generally smaller for the upward case, that is, when the radiances are measured from a satellite. However, for a rather typical cirrus cloud which has an optical depth of unity, say, the correction to the emittance is still significant. As the effect in this case is due largely to multiple scattering, it becomes greatest when the optical depth is about

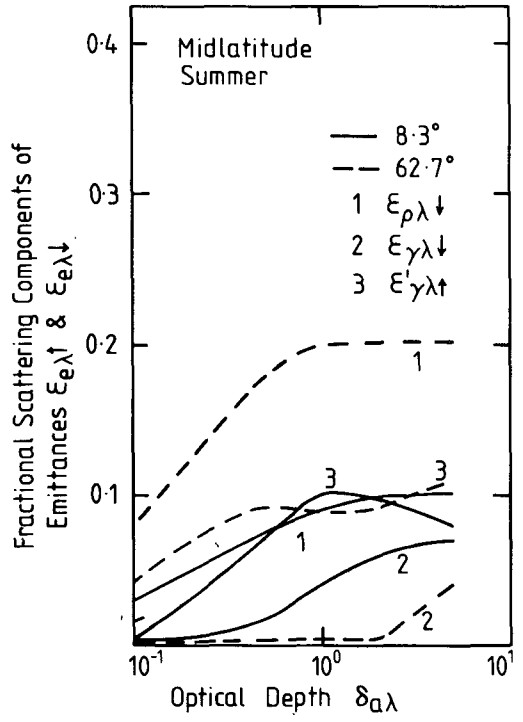

FIG. 8. As in Fig. 7 except for a midlatitude model atmosphere.

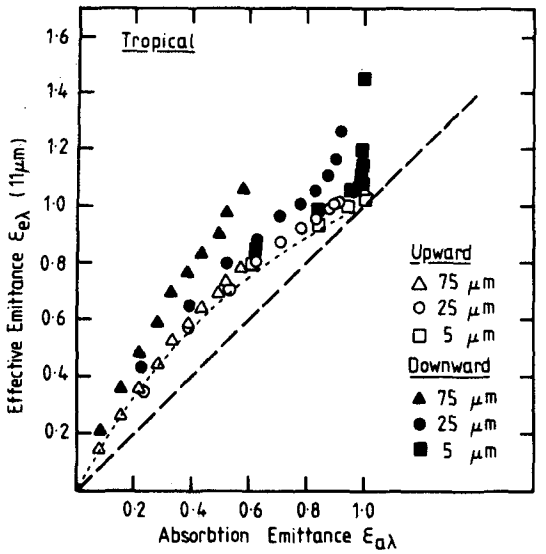

FIG. 9. The 11 μm flux emittance as a function of beam "absorption emittance" for both upward and downward directions and for the three case studies indicated. The calculations were performed for a high cloud positioned in a model tropical atmosphere. The three different sets of points represent the three different ice cylinder radii, as given in Table 1. Dashed line: curve for $\epsilon_{e\lambda} = \epsilon_{a\lambda}$; dotted line: curve for the simple diffuse relation of Eq. (16).

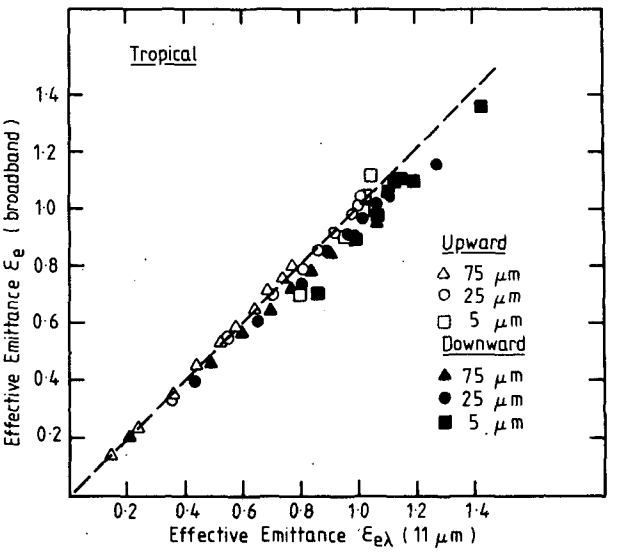

FIG. 11. The relationship between the broadband effective emittance and the narrow band (11 μm) effective emittances for the downward (full) and upward (open points) directions and for a tropical atmosphere. The three different sets of points indicate calculations with the three cylinder radii of Table 1.

unity and then decreases for further increases in optical depth, although this again depends on the angular position of the path of interest.

Figs. 9 and 10 show the effective flux emittance $\epsilon_{e\lambda}$ at 11 μm plotted against the absorption beam emittance $\epsilon_{a\lambda}$. Also shown (dashed curve) is the function $\epsilon^F_{a\lambda}$ [Eq. (16)]. The general features of the results are, first, that the flux emittance is always greater than the beam emittance and, second, that the expression for $\epsilon^F_{a\lambda}$ appears to be a useful approximation, particularly for the upward effective emittance. In the downward case, the large deviations from the curve, particularly in the tropical case, mirror the large influences of reflection. They indicate, as emphasized by Stephens (1980), that the parameterization of cloud radiative properties in terms of an effective emittance becomes difficult for high clouds, at least for the tropical case. The effective emittance, for a given value of $\epsilon_{a\lambda}$, also becomes critical on the particle sizes in the cloud. In actuality a cloud is never monodisperse, so that

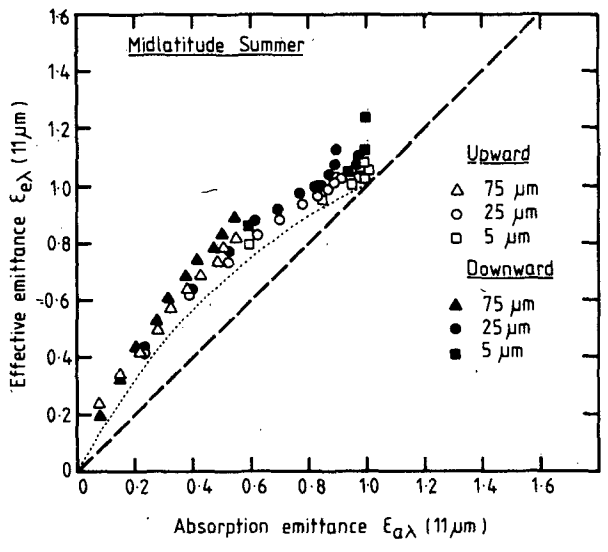

FIG. 10. As in Fig. 9 except for a midlatitude summer atmosphere.

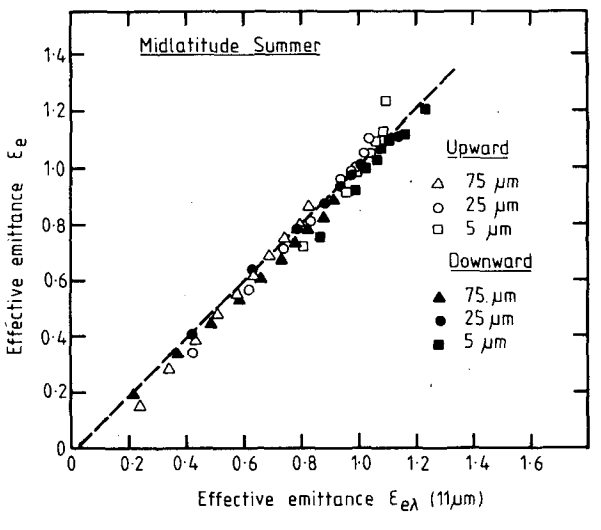

FIG. 12. As in Fig. 11 except for midlatitude summer atmosphere.

the real effective emittance dependence will be a mixture of all three curves. For the midlatitude case, the curve of Eq. (16) gives quite a close representation of $\epsilon_{e\lambda}^{-}$ and $\epsilon_{e\lambda}^{+}$.

The relations between the quantities $\epsilon_{e\lambda}^{+}(\epsilon_{e\lambda}^{-})$ and $\epsilon_{e}^{+}(\epsilon_{e}^{-})$ are shown in Figs. 11 and 12 for the tropical and mid-latitude summer atmospheres, respectively. The correlations between the two quantities are remarkably good; thus, the 11 μm effective flux emittance gives a good representation for the broad-band effective flux emittance. Note that these quantities still include the large reflectances in the tropical case, but as they *both* include such effects, the dependence of ϵ_e on $\epsilon_{e\lambda}$ is still quite linear.

6. Discussion

At the present level of accuracy of the insertion of infrared cloud properties into dynamical or climate models, the infrared radiative properties of each cloud type (e.g., cirrus) are represented by a single broad-band flux emittance value (e.g., Stephens and Webster, 1979). The results presented here show how the mean beam 11 μm emittance value from a program (say) of satellite or ground-based observations could be converted into a representative broad-band flux value for high clouds. For instance, suppose a mean value of the midlatitude effective beam emittance at 11 μm is determined as 0.6 at 0° emergent angle using a mid-cloud temperature. The "effective" optical depth $\delta'_{a\lambda}$ is thus 0.92. From Fig. 8, the scattering components of $\epsilon_{e\lambda}\downarrow$, which are given by the full curves 1 and 2, give a total correction to $\epsilon_{e\lambda}\downarrow$ of $\sim$0.125. The value of $\epsilon_{a\lambda}$ to a first approximation is then 0.475. One can then iterate the calculation if desired, where $\delta_{a\lambda} = 0.64$. This gives a new correction of $\sim$0.10, and a more correct value of $\epsilon_{a\lambda} = 0.5$.

Turning to Fig. 10, a value of 0.5 for $\epsilon_{a\lambda}$ gives a value for $\epsilon_{e\lambda}^{+}$ of 0.8. An equal or slightly lower value can be then used for the broad-band effective flux emittance ϵ_{e}^{+}, as shown by Fig. 12.

The extent to which the results of this article approximate reality can only be gauged at present in terms of two different models of a cirrus cloud. Stephens (1980) computed the (flux) reflectance of a cirrus cloud composed of long ice cylinders and compared this with the reflectance of a cloud of similar optical depth, but composed of ice spheres. In the former case the reflectance was found to be 5%, whereas in the latter it was 3%. Assuming that these values are possible extremes for cirrus clouds, then the maximum error in the computed reflection components of emittance is $\sim$50%. The internal cloud multiple-scattering components depend on the shape of the cloud-particle scattering phase function between 0 and 90° scattering angles. This shape depends more on particle size than particle type, so that the error incurred in calculation of multiple-scattering components will be less than that incurred in the reflection components.

7. Conclusions

The results presented here indicate that it is essential to correct remotely measured beam emittances for the effects of scattering and reflection if a representative value of the absorption beam emittance $\epsilon_{a\lambda}$ is to be found. This emittance can then be used in one of two ways. First, it can be used in a detailed numerical transfer model, using the properties of cirrus clouds (i.e., Table 1) deduced from model calculations to obtain the necessary optical properties. In this case the value of $\epsilon_{a\lambda}$ simply specifies the absorption optical depth, from which the IR extinction optical depth, etc., can be specified. Second, for a less accurate model, the beam emittance $\epsilon_{a\lambda}$ can be converted to a broad-band flux emittance by use of the graphs shown in Figs. 9–12, or to a lesser accuracy, Eq. (16) can be used to specify an approximate broad-band flux emittance.

It should be emphasized that the optical properties of cirrus, which is often an optically thin cloud, are at present inserted very crudely into numerical models. The work discussed here gives a method of calculating IR flux emittances to a reasonable accuracy from experimental results.

Approximate methods have been developed by Platt (1979) to deal with scattering and reflection of IR radiation in a combined lidar and radiometric project. These methods give the same order of magnitudes to within 1 or 2% as in the present work for midlatitude situations (e.g., Figs. 6 and 8). It is apparent from the present study that such corrections are even larger for scattering in a tropical atmosphere.

Acknowledgments. This research has been supported in part by the Air Force Geophysical Laboratory, AFSC, under Contract F 19628-78-C-0207 and in part by Office of Naval Research under Contract N00014-C-0793.

APPENDIX

List of Symbols

ϵ_{e}^{-}	upward effective broadband flux emittance
ϵ_{e}^{+}	downward effective broadband flux emittance
$\epsilon_{e\lambda}^{-}$, $\epsilon_{e\lambda}^{+}$	corresponding narrow-band (11 μm) quantities
$\epsilon_{e}\downarrow$	upward effective broadband beam emittance (at angle θ)

$\epsilon_e\uparrow$ downward effective broadband beam emittance (at angle θ)

$\epsilon_{e\lambda}\downarrow$, $\epsilon_{e\lambda}\uparrow$ corresponding narrow-band quantities

$\epsilon_{a\lambda}$ narrow band (absorption) emittance

M^+, M^- upward and downward flux densities

L^+, L^- upward and downward narrow band beam radiances (at angle θ)

T_b temperature at cloud base

T_t temperature at cloud top

$\bar{T}$ mid-cloud temperature

$\bar{L}_B$ radiance at mid-cloud temperature

$L_B(T)$ narrow-band blackbody radiance at temperature T

$\epsilon^F_{a\lambda}$ narrow-band flux (absorption) emittance

$\delta_{a\lambda}$ absorption component of the optical depth

ρ' components of downward (upward) radiance at all angles 0–90° which are reflected into the upward (downward) direction at zenith angle θ, expressed as a fraction of L_1^+

ρ fraction of upward (downward) radiance L_2^- (L_1^+) which is reflected downward (upward) out of the cloud

γ fraction of upward (downward) radiance L_2^- (L_1^+) which is multiply scattered forward out of the beam direction θ

$\epsilon_{\rho\lambda}\uparrow(\downarrow)$ components of narrow band effective emittances $\epsilon_{e\lambda}\uparrow(\downarrow)$ which are due to reflection

$\epsilon_{\gamma\lambda}\uparrow(\downarrow)$ components of narrow-band effective emittances $\epsilon_{e\lambda}\uparrow(\downarrow)$ which are due to forward and multiple scattering

n number of levels in which the atmosphere is divided (from $n = 1$ to $N + 1$), increasing downward from the top of the atmosphere.

REFERENCES

Cox, S. K., 1976: Observation of cloud infrared effective emissivity. *J. Atmos. Sci.*, **33**, 287–289.

McClatchey, R. A., R. W. Fenn, J. E. Selby, F. E. Volz and J. S. Goring, 1972: *Optical Properties of the Atmosphere*, 3rd ed. AFCRL-72-0497, Air Force Cambridge Research Labs., 107 pp.

Paltridge, G. W., and C. M. R. Platt, 1976: *Radiative Processes in Meteorology and Climatology*. Elsevier, 318 pp.

Platt, C. M. R., 1979: Remote sounding of high clouds: I. Calculation of visible and infrared optical properties from lidar and radiometer measurements. *J. Appl. Meteor.*, **18**, 1130–1143.

——, and A. C. Dilley, 1979: Remote sounding of high clouds: II. Emissivity of cirrostratus. *J. Appl. Meteor.*, **18**, 1144–1150.

Reynolds, D. W., and T. H. Vonder Haar, 1977: A bi-spectral method for estimating cirrus cloud-top heights. *J. Appl. Meteor.*, **12**, 1213–1216.

Shenk, W. E., and R. J. Curran, 1973: A multi-spectral method for estimating cirrus cloud top heights. *J. Appl. Meteor.*, **12**, 1213–1216.

Stephens, G. L., 1976: The transfer of radiation through vertically non-uniform stratocumulus water clouds. *Contrib. Atmos. Phys.*, **49**, 237–253.

——, 1978: Radiation profiles in extended water clouds. I: Theory. *J. Atmos. Sci.*, **35**, 2111–2122.

——, 1980: Radiative properties of cirrus clouds in the infrared region. *J. Atmos. Sci.*, **37**, 435–446.

——, and P. J. Webster, 1979: Sensitivity of radiative forcing to variable cloud and moisture. *J. Atmos. Sci.*, **36**, 1542–1556.

Yamamoto, G., M. Tanaka and S. Asano, 1970: Radiative transfer in water clouds in the infrared region. *J. Atmos. Sci.*, **27**, 282–292.